

INSIDE-OUT PLANET FORMATION

SOURAV CHATTERJEE

Department of Astronomy, University of Florida, Gainesville, FL 32611, USA
s.chatterjee@astro.ufl.edu

JONATHAN C. TAN

Departments of Astronomy & Physics, University of Florida, Gainesville, FL 32611, USA
jt@astro.ufl.edu

Draft version October 31, 2013

ABSTRACT

The compact multi-transiting planet systems discovered by *Kepler* challenge planet formation theories. Formation *in situ* from disks with radial mass surface density, Σ , profiles similar to the minimum mass solar nebula (MMSN) but boosted in normalization by factors $\gtrsim 10$ has been suggested. We propose that a more natural way to create these planets in the inner disk is formation sequentially from the inside-out via creation of successive gravitationally unstable rings fed from a continuous stream of small (\sim cm–m size) “pebbles”, drifting inwards via gas drag. Pebbles collect at the pressure maximum associated with the transition from a magneto-rotational instability (MRI)-inactive (“dead zone”) region to an inner MRI-active zone. A pebble ring builds up until it either becomes gravitationally unstable to form an $\sim 1 M_{\oplus}$ planet directly or induces gradual planet formation via core accretion. The planet may undergo Type I migration into the active region, allowing a new pebble ring and planet to form behind it. Alternatively if migration is inefficient, the planet may continue to accrete from the disk until it becomes massive enough to isolate itself from the accretion flow. A variety of densities may result depending on the relative importance of residual gas accretion as the planet approaches its isolation mass. The process can repeat with a new pebble ring gathering at the new pressure maximum associated with the retreating dead zone boundary. Our simple analytical model for this scenario of inside-out planet formation yields planetary masses, relative mass scalings with orbital radius, and minimum orbital separations consistent with those seen by *Kepler*. It provides an explanation of how massive planets can form with tightly-packed and well-aligned system architectures, starting from typical protoplanetary disk properties.

Subject headings: methods: analytical — planets and satellites: formation — planets and satellites: general — protoplanetary disks

1. INTRODUCTION

A striking property of the *Kepler*-detected planet candidates (KPC) is the existence of multi-transiting systems with tightly-packed inner planets (STIPs): typically 3–5 planets of radii $\sim 1 - 10 R_{\oplus}$ in short-period (1–100d) orbits (Fang & Margot 2012). While short-period giant planets can be explained via planet-planet scattering followed by tidal circularization (Rasio & Ford 1996; Chatterjee et al. 2008; Nagasawa & Ida 2011), this mechanism cannot produce the low dispersion ($\lesssim 3^{\circ}$) in orbital inclinations of STIPs. Their well-aligned orbits imply either formation *in situ* within a disk or formation at larger distances followed by inward migration within a gas disk. The migration scenario has been discussed by, for example, Kley & Nelson (2012): it tends to produce planetary orbits that are trapped near low-order mean motion resonances. However, such pile-ups of orbits near resonances do not appear to be a particular feature of the KPCs, so other mechanisms would then be needed to move planets away from resonance (e.g., Lithwick & Wu 2012; Rein 2012; Batygin & Morbidelli 2013).

Formation *in situ* faces the problem of concentrating a large mass of solids in the inner disk. Chiang & Laughlin (2013) used the observed distribution of KPCs to construct a Σ profile of a typical disk that would

form such planets, finding it has significantly more solids within ~ 1 AU than the MMSN. They then discussed several implications of forming planets from such a disk. Hansen & Murray (2012, 2013) proposed this concentration ($\sim 20 M_{\oplus}$ inside 1 AU) is achieved via migration of small bodies to form an inner enriched disk. They then considered a standard model for planet formation via oligarchic growth from such a disk.

Here we present an alternative model involving *simultaneous* migration of small (\sim cm–m) solids (hereafter “pebbles”), and planet formation at the location where these pebbles are deposited. Inward migration of pebbles occurs via gas drag due to the disk’s radial pressure gradient — long recognized as part of the so called “meter-size barrier” for planetesimal formation (Weidenschilling 1977; Youdin & Kenyon 2013). However, although this inhibits planet formation in most of the disk, we argue it is key for enabling close-in massive planet formation.

In Section 2 we describe our proposed scenario and present a simple analytical model to calculate the predicted planetary masses, mass–orbital distance relation, and minimum planet-planet separations. In Section 3 we compare the predicted planetary properties with the observed *Kepler* systems. Finally, in Section 4 we summarize and discuss implications of our model, as well as identifying caveats that can be tested via future numerical

simulations.

2. OVERVIEW OF THEORETICAL MODEL

A schematic overview of the model is presented in Figure 1, involving four basic stages: (i) Pebble formation and drift to the inner disk; (ii) Pebble ring formation at the pressure maximum associated with dead zone inner boundary; (iii) Planet formation from the pebble ring leading to gap opening and viscous clearing of the inner disk; (iv) Dead zone retreat and formation of a new pebble ring that can lead to subsequent planet formation. These stages are described in more detail below.

2.1. Pebble Formation and Drift to the Inner Disk

Consider an accretion disk of total mass M , composed of gas (M_g) and solids (M_s). We class solids in two types: (1) \lesssim sub-mm dust grains (M_d), perfectly coupled to gas; (2) \gtrsim 1 cm “pebbles” (M_p) that feel significant gas drag. Thus $M_s = M_d + M_p$. The disk is remnant material from star formation with interstellar composition, i.e., $M_s = f_s M_g$ with $f_s \simeq 0.01$.

We will consider a Shakura-Sunyaev alpha-disk model for the protoplanetary disk (Shakura & Sunyaev 1973). The viscosity parameter $\alpha \equiv 0.001\alpha_{-3} = \nu/(c_s H)$, is expected to be $\sim 10^{-2}$ in MRI-active regions, but at least an order of magnitude smaller in the dead zone, where the ionization fraction is too small for the magnetic field to couple to the gas. For example, Dzyurkevich et al. (2010) find $\alpha \sim 10^{-4} - 10^{-3}$ set by diffusion of the mean magnetic field from the active region into the dead zone. Values of α of this order may also result from damping and shocking of spiral density waves that are excited by a planet that is already present in the inner region of the disk (Goodman & Rafikov 2001). While MRI-active disk surface layers may be expected above and below the dead zone (although even here, suppression of the MRI by the global magnetic fields associated with a disk wind remains a possibility; G. Lesur, private communication), here we are concerned with mid-plane properties, where pebbles will have settled.

For a steady, thin, active accretion disk, the mid-plane properties such as pressure (P), temperature (T), sound speed (c_s) can be derived as a function of the basic disk properties including the accretion rate (\dot{m}), disk composition, opacity, and assumed α viscosity (for a detailed discussion and derivation of the structure of alpha-disks see, e.g., Frank et al. 2002). Following closely the treatment in Frank et al. (2002), we can write the mid-plane pressure as

$$P = \frac{2^{1/2}}{3^{11/10}\pi^{4/5}} \left(\frac{\mu}{k_B}\right)^{2/5} \gamma^{-7/5} \left(\frac{\kappa}{\sigma_{\text{SB}}}\right)^{-1/10} \alpha^{-9/10} \times (Gm_*)^{17/20} (f_r \dot{m})^{4/5} r^{-51/20}, \quad (1)$$

$$P/k_B \rightarrow 1.22 \times 10^{16} \gamma_{1.4}^{-7/5} \kappa_{10}^{-1/10} \alpha_{-3}^{-9/10} \times m_{*,1}^{17/20} (f_r \dot{m}_{-9})^{4/5} r_{\text{AU}}^{-51/20} \text{ K cm}^{-3}$$

where $\mu = 2.33m_{\text{H}} = 3.90 \times 10^{-24}$ g is the mean particle mass (assuming $n_{\text{He}} = 0.2n_{\text{H}_2}$), k_B is Boltzmann’s constant, $\gamma \equiv 1.4\gamma_{1.4}$ is the power law exponent of the barotropic equation of state $P = K\rho^\gamma$ where we have normalized for H_2 with rotational modes excited, σ_{SB} is Stefan-Boltzmann’s constant, $m_* \equiv m_{*,1}M_\odot$ is the stellar mass, $\kappa \equiv \kappa_{10}10 \text{ cm}^2 \text{ g}^{-1}$ is disk opacity (normalized

to expected protoplanetary disk values, e.g., Wood et al. 2002), $f_r \equiv 1 - \sqrt{r_*/r}$, (where r_* is stellar radius), and $\dot{m} \equiv \dot{m}_{-9}10^{-9} M_\odot \text{ yr}^{-1}$ is the accretion rate. We have normalized \dot{m} to expected protoplanetary disk values, although these show wide dispersion and may also individually vary over time, i.e., possible accretion bursts superposed on longer term decline (e.g., Williams & Cieza 2011).

Similarly, the density, $\rho = \gamma P c_s^{-2}$, in the disk mid-plane is given by

$$\rho = \frac{2^{3/2}}{3^{13/10}\pi^{2/5}} \left(\frac{\mu}{\gamma k_B}\right)^{6/5} \left(\frac{\kappa}{\sigma_{\text{SB}}}\right)^{-3/10} \alpha^{-7/10} \times (Gm_*)^{11/20} (f_r \dot{m})^{2/5} r^{-33/20}, \quad (2)$$

$$\rightarrow 1.87 \times 10^{-10} \gamma_{1.4}^{-6/5} \kappa_{10}^{-3/10} \alpha_{-3}^{-7/10} \times m_{*,1}^{11/20} (f_r \dot{m}_{-9})^{2/5} r_{\text{AU}}^{-33/20} \text{ g cm}^{-3}$$

(where this fiducial density corresponds to a number density of H_2 molecules of $n_{\text{H}_2} = 4.00 \times 10^{13} \text{ cm}^{-3}$). It then follows that the disk mid-plane sound speed is

$$c_s = \frac{3^{1/10}}{2^{1/2}\pi^{1/5}} \left(\frac{\mu}{\gamma k_B}\right)^{-2/5} \left(\frac{\kappa}{\sigma_{\text{SB}}}\right)^{1/10} \alpha^{-1/10} \times (f_r \dot{m})^{1/5} (Gm_*)^{3/20} r^{-9/20} \quad (3)$$

$$\rightarrow 1.12 \kappa_{10}^{1/10} \gamma_{1.4}^{2/5} \alpha_{-3}^{-1/10} m_{*,1}^{3/20} (f_r \dot{m}_{-9})^{1/5} r_{\text{AU}}^{-9/20} \text{ km s}^{-1},$$

and the disk mid-plane temperature is

$$T = \frac{3^{1/5}}{2\pi^{2/5}} \left(\frac{\mu}{\gamma k_B}\right)^{1/5} \left(\frac{\kappa}{\sigma_{\text{SB}}}\right)^{1/5} \alpha^{-1/5} \times (Gm_*)^{3/10} (f_r \dot{m})^{2/5} r^{-9/10}, \quad (4)$$

$$\rightarrow 254 \gamma_{1.4}^{-1/5} \kappa_{10}^{1/5} \alpha_{-3}^{-1/5} m_{*,1}^{3/10} (f_r \dot{m}_{-9})^{2/5} r_{\text{AU}}^{-9/10} \text{ K}.$$

Disk solids grow from dust grains to pebbles at rate $\dot{M}_p = -\dot{M}_d$ set by coagulation of small grains into larger ones—a complicated process expected to depend on grain structure and composition (e.g., Blum 2010). There is thus a radially-varying source term for pebbles, dependent on dust grain number density. We will see later that we will mostly be concerned with the supply of pebbles forming at locations $r \sim 10 \text{ AU}$.

A decreasing pressure gradient in the disk (Equation 1) causes gas to orbit at slightly sub-Keplerian speeds. Pebbles of mass m_p and radius $a_p \equiv a_{p,1} \text{ cm}$, whose orbits are not affected by this pressure gradient due to low coupling with gas, have relative velocities with respect to the gas of magnitude $v_\Delta \simeq t_{\text{fric}} v_{r,p} v_K / (2r)$ (Weidenschilling 1977; Takeuchi & Lin 2002; Armitage 2007). Here t_{fric} is the frictional timescale, $v_{r,p}$ is the radial drift speed of the pebble and v_K is the Keplerian speed. The frictional time scale is defined as $t_{\text{fric}} \equiv m_p v_\Delta / |F_D|$, where F_D is the drag force. The drag force is $|F_D| = (1/2)C_D \pi a_p^2 \rho v_\Delta^2$, where C_D is the drag coefficient. The Epstein regime of drag applies when $a_p < (9/4)\lambda$, where λ is the mean free path of molecules, given by

$$\lambda = \frac{1}{n_{\text{H}_2} \sigma_{\text{H}_2}} \quad (5)$$

$$= 12.5 \gamma_{1.4}^{-6/5} \kappa_{10}^{3/10} \alpha_{-3}^{7/10} m_{*,1}^{-11/20} (f_r \dot{m}_{-9})^{-2/5} r_{\text{AU}}^{33/20} \text{ cm},$$

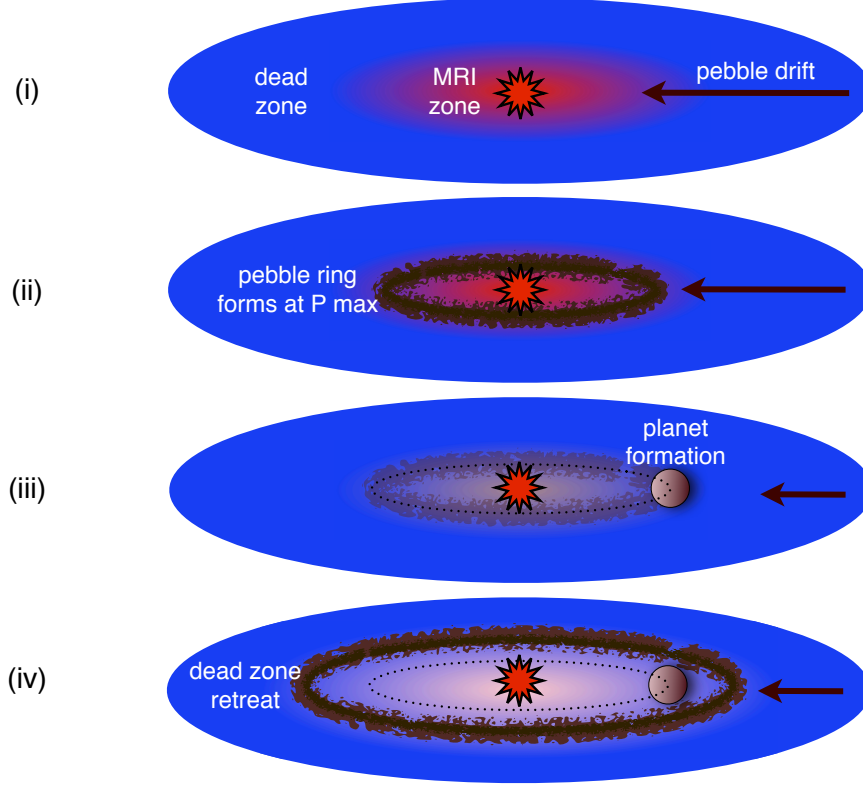


FIG. 1.— Schematic overview of the stages of the inside-out planet formation scenario. (i) Pebble formation and drift to the inner disk. Pebbles form via dust coagulation in the protoplanetary disk. Those with \sim cm–m sizes attain high radial drift velocities and quickly reach the dead zone inner boundary, where they become trapped at the pressure maximum. (ii) Pebble ring formation. A ring of pebbles gradually builds up over a timescale set by the pebble formation and supply rate from the outer disk. (iii) Planet formation and gap opening. A planet forms either via gravitational (Toomre) instability of the ring or via core accretion. In both cases, a gradual accumulation of the bulk of the ring mass into a single planet is anticipated. In the case of gravitational instability, this ring mass, once organized into a single planet, may be larger than the mass needed to open a gap in the gas disk. For core accretion, the final planet mass may be limited by such gap opening. In both cases, gap opening is soon followed by viscous clearing of the gas disk interior to the planet’s orbit. (iv) Dead zone retreat and subsequent pebble ring and planet formation. Gap opening and associated viscous clearing of the inner disk allow greater penetration of X-ray photons from the protostar to the disk mid-plane, increasing its ionization fraction and thus activating the magneto-rotational instability (MRI). The inactive dead zone retreats, along with the pressure maximum associated with its inner boundary. A new pebble ring starts to form at this location that can form a new planet. This cycle repeats leading to sequential formation of a planetary system from the inside-out.

where we have adopted $\sigma_{\text{H}_2} = 2 \times 10^{-15} \text{ cm}^2$. In this regime $C_D = 2^{9/2} c_s / (3\sqrt{\pi} v_\Delta)$. As discussed by Armitage (2007), the pebble inward radial drift velocity $v_{r,p}$, depends on pebble size and the disk’s pressure profile $P = P_0(r/r_0)^{-k_P}$, and is given by

$$\begin{aligned}
 v_{r,p} &\simeq \frac{-k_P (c_s/v_K)^2}{\tau_{\text{fric}} + \tau_{\text{fric}}^{-1}} v_K \\
 |v_{r,p}| &\simeq \frac{3^{1/5}}{2\pi^{2/5}} f_\tau k_P \left(\frac{\mu}{\gamma k_B}\right)^{-4/5} \left(\frac{\kappa}{\sigma_{\text{SB}}}\right)^{1/5} \alpha^{-1/5} \\
 &\times (Gm_*)^{-1/5} (f_r \dot{m})^{2/5} r^{-2/5} \\
 &\rightarrow 0.108 f_\tau \gamma_{1.4}^{4/5} \kappa_{10}^{1/5} \alpha_{-3}^{-1/5} m_{*,1}^{-1/5} \\
 &\times (f_r \dot{m}_{-9})^{2/5} r_{\text{AU}}^{-2/5} \text{ km s}^{-1}.
 \end{aligned} \tag{6}$$

where $\tau_{\text{fric}} \equiv \Omega_K t_{\text{fric}}$ is the normalized pebble frictional time, where $\Omega_K = (GM/r^3)^{1/2}$, and $f_\tau \equiv (\tau_{\text{fric}} + \tau_{\text{fric}}^{-1})^{-1}$. For the alpha disk given by Equation 1, $k_P = 51/20 = 2.55$.

The radial drift timescale is then

$$\begin{aligned}
 t_{\text{drift}} &\equiv \frac{r}{|v_{r,p}|} \\
 &= \frac{2\pi^{2/5}}{3^{1/5} f_\tau k_P} \left(\frac{\mu}{\gamma k_B}\right)^{4/5} \left(\frac{\kappa}{\sigma_{\text{SB}}}\right)^{-1/5} \alpha^{1/5} \\
 &\times (Gm_*)^{1/5} (f_r \dot{m})^{-2/5} r^{7/5} \\
 &\rightarrow 43.9 f_\tau^{-1} \gamma_{1.4}^{-4/5} \kappa_{10}^{-1/5} \alpha_{-3}^{1/5} m_{*,1}^{1/5} (f_r \dot{m}_{-9})^{-2/5} r_{\text{AU}}^{7/5} \text{ yr}.
 \end{aligned} \tag{7}$$

If $\tau_{\text{fric}} \sim \mathcal{O}(1)$, then t_{drift} for pebbles is much shorter than the disk lifetime, expected to be $\gtrsim 1$ Myr (Williams & Cieza 2011).

Growing from small dust grains, pebbles will first be in the Epstein drag regime. In this case

$$\begin{aligned}
 \tau_{\text{fric}} &= \frac{3^{6/5} \pi^{11/10}}{2^{5/2}} \rho_p a_p \left(\frac{\mu}{\gamma k_B}\right)^{-4/5} \left(\frac{\kappa}{\sigma_{\text{SB}}}\right)^{1/5} \alpha^{4/5} \\
 &\times (Gm_*)^{-1/5} (f_r \dot{m})^{-3/5} r^{3/5} \\
 &\rightarrow 0.0178 a_{p,1} \rho_{p,3} \gamma_{1.4}^{4/5} \kappa_{10}^{1/5} \alpha_{-3}^{-1/5} m_{*,1}^{-1/5} (f_r \dot{m}_{-9})^{-3/5} r_{\text{AU}}^{3/5},
 \end{aligned} \tag{8}$$

where $\rho_p \equiv \rho_{p,3} 3 \text{ g cm}^{-3}$ is the pebble density. In this limit where $\tau_{\text{fric}} \ll 1$, $f_r \rightarrow \tau_{\text{fric}}$. However, the process of radial drift of pebbles should lead to their rapid growth as they sweep up smaller dust grains, especially in colder outer regions of the disk where grains still retain their ice mantles. In the CQ Tau protoplanetary disk, Trotta et al. (2013) have derived maximum “grain” sizes of a few mm at 80 AU, increasing to a few cm in the inner 40 AU. If growth is efficient, then pebbles may reach sizes associated with the maximum radial drift speed, i.e. for $\tau_{\text{fric}} = 1$. Equation 8 can be rearranged to yield an expression for pebble size:

$$\begin{aligned} a_p &= \frac{2^{5/2}}{3^{6/5} \pi^{11/10}} \frac{\tau_{\text{fric}}}{\rho_p} \left(\frac{\mu}{\gamma k_B} \right)^{4/5} \left(\frac{\kappa}{\sigma_{\text{SB}}} \right)^{-1/5} \alpha^{-4/5} \\ &\times (Gm_*)^{1/5} (f_r \dot{m})^{3/5} r^{-3/5} \\ &\rightarrow 56.2 \rho_{p,3}^{-1} \tau_{\text{fric}}^{-4/5} \gamma_{1.4}^{-1/5} \kappa_{10}^{-4/5} \alpha_{-3}^{-4/5} \\ &\times m_{*,1}^{1/5} (f_r \dot{m}_{-9})^{3/5} r_{\text{AU}}^{-3/5} \text{ cm}, \end{aligned} \quad (9)$$

The condition to be in the Epstein drag regime, $4a_p/(9\lambda) < 1$, can be evaluated via

$$\frac{4a_p}{9\lambda} = 1.99 \rho_{p,3}^{-1} \tau_{\text{fric}}^{2/5} \gamma_{1.4}^{2/5} \kappa_{10}^{-1/2} \alpha_{-3}^{-3/2} m_{*,1}^{3/4} (f_r \dot{m}_{-9}) r_{\text{AU}}^{-9/4}. \quad (10)$$

We see that for the fiducial disk parameters it is satisfied for $r_{\text{AU}} > 1.36 \tau_{\text{fric}}^{4/9}$, i.e. for the bulk of the feeding zone that we expect to be relevant for planet formation (§2.4).

Thus pebbles, growing from small sizes, will first be in the Epstein drag regime and will drift inwards on relatively short timescales. As they enter denser regions of the disk, they will enter the Stokes drag regime, but continue drifting inwards. While pebbles that have $\tau_{\text{fric}} = 1$ reach the inner disk the fastest, given the generally short values of t_{drift} , we expect the delivered material to actually have a relatively broad distribution of sizes and thus also radial drift speeds. We conclude, like Hansen & Murray (2012), that radial pebble migration can provide a large reservoir of solids to build inner short period planets. Given the short drift timescales, the rate limiting step for the supply of pebbles to the inner dead zone boundary is likely to be their formation rate via dust coagulation in the outer disk.

2.2. Pebble Ring Formation at Inner Disk Pressure Maximum

We assume there is an inner-disk location, r_0 , where, moving inwards, gas pressure declines rapidly from a local maximum, leading to accumulation of pebbles. We expect the mechanism responsible for initially creating this central “pressure hole” is the transition from an outer MRI-inactive, dead zone, region to an inner active region. We see from Equation 1, that the pressure scales as $P \propto \alpha^{-9/10}$, so as α rapidly increases on leaving the inner dead zone boundary, mid-plane pressure decreases almost as rapidly. Note that although κ , set by dust opacity, is a function of local disk properties (i.e. density and temperature), it is not expected to vary strongly in this transition region. Moreover, P has a very weak dependence on κ . This analytical expectation for the existence of a pressure maximum associated with the inner dead zone boundary is also seen in the results from numerical simulation by Dzyurkevich et al. (2010).

Depending on disk properties such as \dot{m} and α and stellar X-ray luminosity, L_X , the location of the inner dead zone boundary in the disk mid-plane, i.e. the location where the ionization fraction reaches a certain critical value, is likely to be set either by thermal ionization of alkali metals at $T \sim 1200 \text{ K}$ (Umebayashi & Nakano 1988) or by penetration of protostellar X-rays that are produced from flares associated with magnetic activity both near the stellar surface and possibly also from a disk corona. The X-ray luminosity of young stars is thus, by its nature, highly variable and so the radial location of the dead zone inner boundary could also fluctuate, depending on the timescale for MRI turbulence to develop in response to a change in ionization.

From Equation 4, we see that the temperature of 1200 K for thermal ionization of alkali metals is achieved at

$$r_{1200\text{K}} = 0.178 \gamma_{1.4}^{-2/9} \kappa_{10}^{2/9} \alpha_{-3}^{-2/9} m_{*,1}^{1/3} (f_r \dot{m}_{-9})^{4/9} \text{ AU}. \quad (11)$$

If there is efficient extraction of accretion power as mechanical luminosity of a disk wind, then the disk at a given radius will be cooler than predicted by Equation 4. For example, in the disk models of Zhang et al. (2013) including this effect of disk winds causes a given temperature zone to be about 20% closer to the star compared to models without winds. These models also show that as κ begins to decrease at $T \gtrsim 1400 \text{ K}$, the disk temperature is kept relatively constant over a factor of several in radius. Given the uncertainties in dust composition and the temperature of dust destruction, it is possible that opacity reduction may begin at $T \simeq 1200 \text{ K}$, thus keeping the disk at this temperature to radii that are factors of several smaller than predicted by Equation 11.

More detailed calculations of the thermal and ionization structure of protostellar accretion disks, together with input models for the global magnetic field structure, are needed for accurate prediction of the location of the dead zone inner boundary due to thermal and X-ray ionization. Example calculations of dead zone boundaries have been carried out by Matsumura & Pudritz (2005); Dzyurkevich et al. (2010); Mohanty et al. (2013); Ormel & Okuzumi (2013). For example, in the fiducial model of Mohanty et al. (2013), the dead zone extends inside 0.1 AU, but this is sensitive to model input parameters.

In summary, the dead zone inner boundary in an active accretion disk is likely to be set by thermal ionization of alkali metals, and can be at a small fraction of an AU, depending on the accretion rate. The estimate given by Equation 11 for $r_{1200\text{K}}$, should be regarded as an upper limit, since, both disk wind energy extraction and opacity reduction due to dust destruction, act to reduce the disk mid-plane temperature compared to the value given in Equation 4 at a given location.

Efficient pebble drift from the outer disk together with the strong theoretical expectation of an inner local pressure maximum at the dead zone inner boundary make it likely that a pebble ring will form at this location. We expect and will assume that the global radial drift of pebbles, through the dead zone, to r_0 will overwhelm any mechanism that may be acting to limit the concentration of solids, such as vertical shear instabilities (e.g., Weidenschilling 1980; Youdin & Shu 2002), turbulence induced by streaming instabilities (Bai & Stone 2010a,b),

or Rossby wave instabilities (e.g., Meheut et al. 2012; Lyra & Mac Low 2012).

Now we examine the condition that must be satisfied to ensure that after pebbles are delivered to r_0 , they are trapped at the pressure maxima, instead of being carried further inwards by the radial inward flow of gas. The positive pressure gradient associated with the dead zone inner edge will induce a net outward radial drift velocity of pebbles with respect to gas, and this velocity needs to be larger than the inward radial flow of gas due to viscous accretion, $v_{r,g}$, given by

$$\begin{aligned} v_{r,g} &= -3\nu/(2f_r r) \\ |v_{r,g}| &= \frac{3^{6/5}}{4\pi^{2/5}} \left(\frac{\mu}{\gamma k_B}\right)^{-4/5} \left(\frac{\kappa}{\sigma_{\text{SB}}}\right)^{1/5} \alpha^{4/5} \\ &\quad \times (Gm_*)^{-1/5} f_r^{-3/5} \dot{m}^{2/5} r^{-2/5} \\ &\rightarrow 6.34 \gamma_{1.4}^{4/5} \kappa_{10}^{1/5} \alpha_{-3}^{4/5} m_{*,1}^{-1/5} f_r^{-3/5} \dot{m}_{-9}^{2/5} r_{\text{AU}}^{-2/5} \text{ cm s}^{-1}. \end{aligned} \quad (12)$$

Describing the edge pressure gradient by a power law $\propto r^{-k_{P,\text{edge}}}$, we expect $k_{P,\text{edge}} < -k_P \rightarrow -2.55$ and will normalize to a fiducial value of -10. Then the condition $v_{r,p} > |v_{r,g}|$ implies $\tau_{\text{fric}} > 3\alpha/(2k_{P,\text{edge}} f_r)$. In the Epstein drag regime with $\tau_{\text{fric}} \ll 1$, then Equations 8 and 11 imply

$$a_p > 0.0237 \rho_{p,3}^{-1} k_{P,\text{edge},-10}^{2/3} \gamma_{1.4}^{-1/3} \kappa_{10}^{1/3} \alpha_{-3}^{1/3} f_r^{-2/3} \dot{m}_{-9}^{1/3} \text{ cm}. \quad (13)$$

Thus the bulk of the pebble population delivered to the dead zone inner edge will be trapped near the pressure maximum. The surface density of pebbles will continue to grow. Next we discuss the implications for planet formation from such a ring.

2.3. Planet Formation

We consider two planet formation mechanisms: (1) gravitational instability; (2) core accretion.

2.3.1. Via Gravitational Instability

Planets may form via Toomre ring instability of a pebble-dominated region with $\Sigma(r_0) \simeq \Sigma_p$. With reference to the Toomre stability parameter for a gaseous disk, instability develops when $Q \equiv \Omega_K \sigma_p / (\pi G \Sigma_p) \lesssim 1$, where σ_p is pebble velocity dispersion. If the mass surface densities of pebbles is much greater than that of gas, i.e. $\Sigma_p \gg \Sigma_g$, as is shown below, then their velocity dispersion will be little affected by any MRI-induced turbulence that is in the vicinity of the dead zone boundary and we expect $\sigma_p < c_s$.

We assume $\sigma_p = \phi_\sigma |v_{r,p}(\tau_{\text{fric}} = 1)|$, with $\phi_\sigma \sim \mathcal{O}(1)$, i.e. pebble velocity dispersion is similar to the maximum drift speed just before delivery to r_0 . This inertial limit is expected if there is a sharp decrease in pressure at the inner dead zone boundary and is thus an upper limit. It is also an upper limit given that we expect a wide mass spectrum of pebbles to be delivered, that will have a range of values of τ_{fric} . From equations 8 and 11, we see that for fiducial parameters, \sim cm-sized pebbles reach the dead zone inner boundary (if set by thermal ionization) via Epstein drag with $\tau_{\text{fric}} \sim 0.01$. Larger, 10-cm-sized pebbles would be in the Stokes drag regime with Reynolds numbers $\text{Re} = 2a_p v_\Delta / \nu_{\text{mol}} < 1$, where ν_{mol} is the microscopic (molecular) viscosity $\nu_{\text{mol}} \simeq \lambda c_s \simeq$

$c_s/(n_{\text{H}_2} \sigma_{\text{H}_2})$ and $\sigma_{\text{H}_2} \simeq 2 \times 10^{-15} \text{ cm}^2$. In this case, $C_D = 24\text{Re}^{-1}$ and

$$\begin{aligned} \tau_{\text{fric}} &\rightarrow 0.101 a_{p,10}^2 \rho_{p,3} \gamma_{1.4}^{-2/5} \kappa_{10}^{-1/10} \alpha_{-3}^{1/10} \\ &\quad \times m_{*,1}^{7/20} (f_r \dot{m}_{-9})^{-1/5} r_{\text{AU}}^{-21/20}, \end{aligned} \quad (14)$$

using

$$\begin{aligned} \text{Re} &\rightarrow 9.65 a_{p,10} \frac{\tau_{\text{fric}}}{\tau_{\text{fric}} + \tau_{\text{fric}}^{-1}} \gamma_{1.4}^{-4/5} \kappa_{10}^{1/5} \alpha_{-3}^{4/5} \\ &\quad \times m_{*,1}^{1/5} (f_r \dot{m}_{-9})^{3/5} r_{\text{AU}}^{-8/5}. \end{aligned} \quad (15)$$

However, note that at the fiducial location of the dead zone inner boundary, given by Equation 11, i.e. 0.178 AU, a 10-cm-sized pebble would have $\tau_{\text{fric}} = 0.62$, implying $\text{Re} \sim 40$, which is a regime described by a different drag coefficient, $C_D = 24\text{Re}^{-0.6}$ ($1 < \text{Re} < 800$), that would predict a value of C_D about 4 times higher than in the $\text{Re} < 1$ regime. We see that an accurate calculation of the mass-averaged value of ϕ_σ of the pebbles delivered to a particular dead zone inner boundary location depends on a model for the size distribution and thus growth of pebbles. Such a calculation is beyond the scope of the present paper, and so for simplicity we adopt a fiducial value of $\phi_\sigma = 0.3$, which will characterize the behavior of the population of pebbles that are being delivered most efficiently by gas drag to the inner disk. We note that once pebbles reach the location of the pressure maximum, r_0 , there are other processes such as continued gas drag and pebble-pebble collisions that can also act to reduce σ_p . On the other hand, excitation of velocity dispersion by interaction with any turbulence present in the gas would tend to increase ϕ_σ .

We thus express the mass surface density of pebbles at the time of development of gravitational instability as

$$\begin{aligned} \Sigma_p &= \frac{\phi_\sigma |v_{r,p}| \Omega_K}{\pi G Q} = \frac{\phi_\sigma k_P c_s^2}{2\pi G Q r} \\ &= \frac{3^{1/5}}{4\pi^{7/5}} \phi_\sigma k_P Q^{-1} \left(\frac{\mu}{\gamma k_B}\right)^{-4/5} \left(\frac{\kappa}{\sigma_{\text{SB}}}\right)^{1/5} \alpha^{-1/5} \\ &\quad \times G^{-7/10} m_*^{3/10} (f_r \dot{m})^{2/5} r^{-19/10} \\ &\rightarrow 1.54 \times 10^3 \phi_{\sigma,0.3} Q^{-1} \gamma_{1.4}^{4/5} \kappa_{10}^{1/5} \alpha_{-3}^{-1/5} \\ &\quad \times m_{*,1}^{3/10} (f_r \dot{m}_{-9})^{2/5} r_{\text{AU}}^{-19/10} \text{ g cm}^{-2}. \end{aligned} \quad (16)$$

The above mass surface density is much higher than that of the gas,

$$\begin{aligned} \Sigma_g &= \frac{2}{3^{6/5} \pi^{3/5}} \left(\frac{\mu}{\gamma k_B}\right)^{4/5} \left(\frac{\kappa}{\sigma_{\text{SB}}}\right)^{-1/5} \alpha^{-4/5} \\ &\quad \times (Gm_*)^{1/5} (f_r \dot{m})^{3/5} r^{-3/5} \\ &\rightarrow 106 \gamma_{1.4}^{-4/5} \kappa_{10}^{-1/5} \alpha_{-3}^{-4/5} m_{*,1}^{1/5} (f_r \dot{m}_{-9})^{3/5} r_{\text{AU}}^{-3/5} \text{ g cm}^{-2}, \end{aligned} \quad (17)$$

with ratio of Σ_p/Σ_g given by:

$$\begin{aligned} \frac{\Sigma_p}{\Sigma_g} &= \frac{3^{7/5}}{8\pi^{4/5}} \frac{k_P \phi_\sigma}{Q} \left(\frac{\mu}{\gamma k_B}\right)^{-8/5} \left(\frac{\kappa}{\sigma_{\text{SB}}}\right)^{2/5} \alpha^{3/5} \\ &\quad \times G^{-9/10} m_*^{1/10} (f_r \dot{m})^{-1/5} r^{-13/10} \\ &\rightarrow 14.5 \phi_{\sigma,0.3} \gamma_{1.4}^{8/5} \kappa_{10}^{2/5} \alpha_{-3}^{3/5} m_{*,1}^{1/10} (f_r \dot{m}_{-9})^{-1/5} r_{\text{AU}}^{-13/10}. \end{aligned} \quad (18)$$

Thus at the time of the development of gravitational instability we do not expect the pebble velocity dispersion to be significantly influenced by that of the gas.

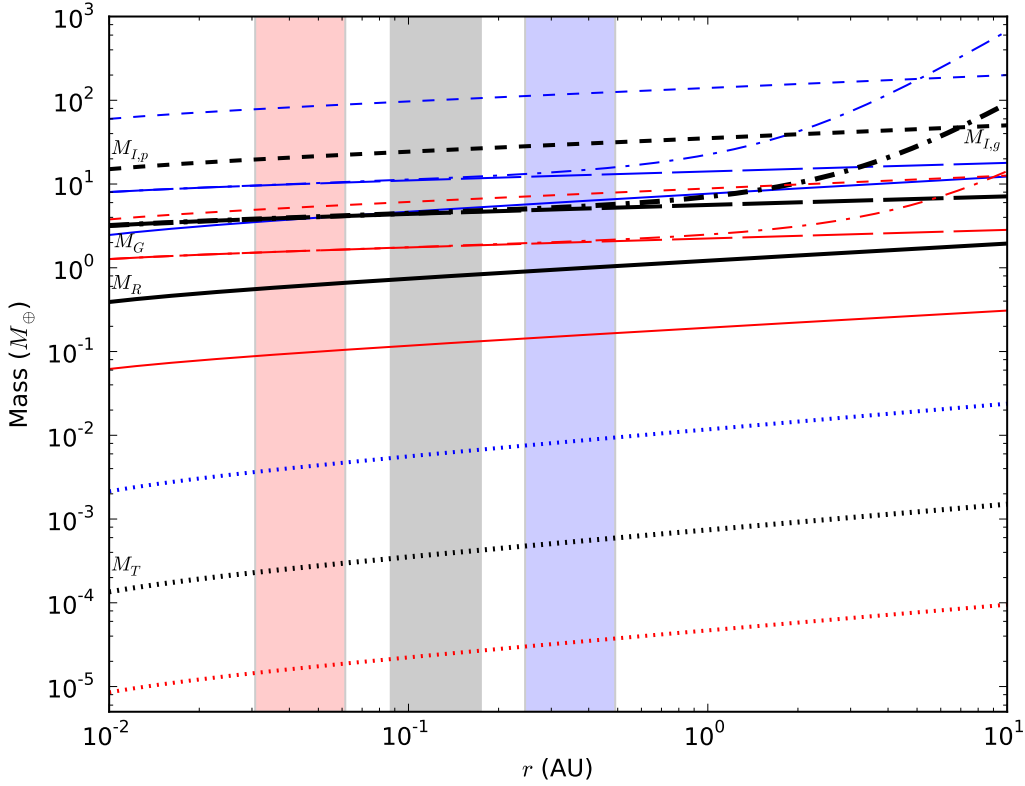


FIG. 2.— Mass scales of planet formation versus distance, r , from star for disks with accretion rate $\dot{m} = 10^{-10}, 10^{-9}, 10^{-8} M_{\odot} \text{ yr}^{-1}$ (red, black, blue lines, respectively). Toomre mass M_T (dotted), Toomre ring mass M_R (solid), gap-opening mass M_G (long-dashed), isolation mass in gas-dominated disk $M_{I,g}$ (dot-dashed), and isolation mass in pebble-dominated disk $M_{I,p}$ (dashed) are shown. The vertical shaded regions indicate the approximate locations for $T = 1200 \text{ K}$, where thermal ionization of alkali metals is expected to become important. Red, black, and blue indicate $\dot{m} = 10^{-10}, 10^{-9}$, and $10^{-8} M_{\odot} \text{ yr}^{-1}$, respectively. The right boundaries in the shaded regions are at $r_{1200\text{K}}$ (the boundaries are at $0.5r_{1200\text{K}}(\dot{m})$). The choice of the left boundaries is somewhat ad-hoc and indicates that the location for a given temperature can be quite uncertain (see text).

The most unstable radial length scale in the pebble ring is $\lambda_T = 2\sigma_p^2/(G\Sigma_p)$. An approximate estimate for the minimum mass associated with this scale is the Toomre mass

$$\begin{aligned}
 M_T &\equiv \Sigma_p \lambda_T^2 = \frac{\pi \phi_{\sigma}^3 k_P^3 Q c_s^6 r^3}{2G^3 m_*^2} \\
 &= \frac{3^{3/5}}{24\pi^{1/5}} \phi_{\sigma}^3 k_P^3 Q \left(\frac{\mu}{\gamma k_B}\right)^{-12/5} \left(\frac{\kappa}{\sigma_{\text{SB}}}\right)^{3/5} \alpha^{-3/5} \\
 &\times G^{-21/10} m_*^{-11/10} (f_r \dot{m})^{6/5} r^{3/10} \\
 &\rightarrow 7.60 \times 10^{-4} \phi_{\sigma,0.3}^3 Q_{1.4}^{12/5} \kappa_{10}^{3/5} \alpha_{-3}^{-3/5} \\
 &\times m_{*,1}^{-11/10} (f_r \dot{m}_{-9})^{6/5} r_{\text{AU}}^{3/10} M_{\oplus}.
 \end{aligned} \tag{19}$$

However, this is likely to be a lower limit on the mass accumulated by gravitational instability. Note that the orbital timescale t_{orb} for the M_T -mass bodies at r_0 is much shorter than t_{drift} . Hence, we expect that the bulk of the ring material will be gathered into a single planet with Toomre “ring mass”

$$M_R \equiv 2\pi r \lambda_T \Sigma_p = 4\pi r \phi_{\sigma}^2 \frac{|v_{r,p}|^2}{G} = \frac{\pi \phi_{\sigma}^2 k_P^2 r^2 c_s^4}{G^2 m_*}$$

$$\begin{aligned}
 &= \frac{3^{2/5} \pi^{1/5}}{2^2} \phi_{\sigma}^2 k_P^2 \left(\frac{\mu}{\gamma k_B}\right)^{-8/5} \left(\frac{\kappa}{\sigma_{\text{SB}}}\right)^{2/5} \alpha^{-2/5} \\
 &\times G^{-7/5} m_*^{-2/5} (f_r \dot{m})^{4/5} r^{1/5} \\
 &\rightarrow 1.23 \phi_{\sigma,0.3}^2 \gamma_{1.4}^{8/5} \kappa_{10}^{2/5} \alpha_{-3}^{-2/5} m_{*,1}^{-2/5} (f_r \dot{m}_{-9})^{4/5} r_{\text{AU}}^{1/5} M_{\oplus}.
 \end{aligned} \tag{20}$$

Figure 2 shows $M_T(r)$ and $M_R(r)$ in disks around a solar-mass star with $\dot{m} = 10^{-10}, 10^{-9}$ and $10^{-8} M_{\odot} \text{ yr}^{-1}$.

The ratio of the ring mass to the Toomre mass is

$$\begin{aligned}
 \frac{M_R}{M_T} &\equiv \frac{4\pi^{2/5}}{3^{1/5}} (\phi_{\sigma} k_P Q)^{-1} \left(\frac{\mu}{\gamma k_B}\right)^{4/5} \left(\frac{\kappa}{\sigma_{\text{SB}}}\right)^{-1/5} \alpha^{1/5} \\
 &\times (G m_*)^{7/10} (f_r \dot{m})^{-2/5} r^{-1/10} \\
 &\rightarrow 1620 \phi_{\sigma,0.3}^{-1} Q^{-1} \gamma_{1.4}^{-4/5} \kappa_{10}^{-1/5} \alpha_{-3}^{1/5} \\
 &\times m_{*,1}^{7/10} (f_r \dot{m}_{-9})^{-2/5} r_{\text{AU}}^{-1/10}.
 \end{aligned} \tag{21}$$

Thus growth to M_R from M_T involves an increase in mass by a large factor. Detailed investigation of this stage requires numerical simulation, but should fall within two limits: (1) Pebble accretion by the first Toomre mass protoplanet; (2) Oligarchic growth from a population of many Toomre mass protoplanets born together at the same orbital radius. In the first case, a ring mass planet

is formed on a near circular orbit from the pebble ring. In the second case, for these relatively low mass protoplanets that are quite close to the central star, strong encounters often lead to physical collisions and strong scattering is not likely. Moreover, the observed low dispersion of orbital inclination angles in the STIPs planets would require this limit to apply.

The planet may continue to grow beyond M_R since it is still embedded in a gaseous disk that is also still delivering pebbles. As discussed below (§2.4), truncating such accretion may require either the planet becoming massive enough to open a gap, or migrating away from the pressure maximum via inward Type I migration (e.g., Menou & Goodman 2004).

2.3.2. Via Core Accretion

Alternatively, planets may form via core accretion from the rich supply of solids in the pebble ring. However, because of difficulties in sticking meter-sized pebbles together, the first step of forming planetesimals likely requires larger-scale streaming instabilities (e.g., Youdin & Goodman 2005) or gathering of material in vortices (e.g., Varnière & Tagger 2006). Collisional runaway growth of a protoplanet may then occur from this planetesimal population. The practical difference between this formation scenario and that involving gravitational instability is that the minimum planet mass is now $\ll M_T$. However, since fiducial values of $M_T \ll M_\oplus$, it is difficult to distinguish these scenarios observationally.

2.4. Migration, Gap Opening, Dead Zone Retreat and Subsequent Planet Formation

Once a planet has formed from the pebble ring, we envisage two potential subsequent evolutionary scenarios: (1) Efficient Type I migration of the planet into the MRI-active region (§2.4.1), followed by formation of another pebble ring and eventually another planet at the dead zone inner boundary, at approximately fixed location in the disk; (2) Inefficient Type I migration and/or rapid growth of the planet to a mass capable of opening a gap in the disk (§2.4.2), followed by dead zone retreat and formation of a new pebble ring and planet further out in the disk. As discussed later in §2.4, the global reservoir of pebbles places constraints on both of these scenarios.

2.4.1. Birth and Migration from a Fixed Parent Pebble Ring

If M_R is smaller than the mass needed to open a gap in the disk, M_G (see §2.4.2), then such a planet will undergo Type I migration (Ward 1997). Detailed analysis of the ultimate fate of a planet undergoing Type I migration is an active area of research (e.g., Paardekooper et al. 2010). The rate and even the direction of migration in the region near the dead-zone-MRI-active-zone boundary will depend on the details of the complicated local density and temperature profiles, which in turn depend on the changes in α and κ . Thus here we simply discuss the expected qualitative behavior of these migrating planets and the implications for such migration on observable planet properties.

For our fiducial disk model ($\Sigma \sim r^{-3/5}$; Equation 17) the co-orbital torque is positive, i.e., the co-orbital torques would result in an outward migration (for a review see Lubow & Ida 2011). If the co-orbital torques are

saturated, torque due to the Lindblad resonances (LR) dominate and result in inward migration of the planet. However, due to the steep r -dependence of the angular momentum of a planet's orbit, the migration rate $\dot{r}_{\text{Type I}}$ decreases with decreasing r for typical disk density profiles. For example, for our fiducial disk model the Type I migration rate due to the LRs for a given planet mass $M_{\text{pl}} \sim M_R$ is $\dot{r}_{\text{Type I}} \sim r^{9/10}$ if $h/R_H < 1$, and $\sim r^{4/5}$ if $h/R_H > 1$, where h is the disk scale height, and $R_H \equiv (M_{\text{pl}}/[3m_*])^{1/3}r$ is the Hill sphere of the migrating planet (Lubow & Ida 2011). As the planet migrates into the MRI active region by crossing r_0 , the dead-zone inner boundary, it finds itself in a disk with much lower $\Sigma_g \sim \alpha^{-4/5}$ (Equation 17) because of the potentially orders of magnitude larger α in the MRI-active region compared to α inside the dead-zone. The low- Σ_g also would result in a low $\dot{r}_{\text{Type I}} \sim \Sigma_g$. The temperature gradient both from the r -dependence and change in κ at the boundary (Equation 4) can also contribute to an outward net torque component on the planet (e.g., Paardekooper & Mellema 2006; Paardekooper et al. 2010).

If there is efficient inward Type I migration of the planet away from the dead zone inner boundary, then conditions may be set up for re-forming a pebble ring at the associated pressure maximum. A whole series of planets may form sequentially at r_0 , which then migrate inwards to form a compact planetary system. If the disk properties (\dot{m} , r_0) are relatively steady, then the resulting planetary masses, compositions and densities may also be quite similar.

The ultimate change in the planetary orbits due to Type I migration will depend on both the rate of migration and the amount of time available for this process. Once inside the MRI-active region, further growth of these planets via accretion appears to be difficult, since (1) pebbles remain trapped at the dead zone inner boundary; (2) the gas is hot ($\gtrsim 1200$ K) and hence harder to accrete. Type I migration may be limited by the time needed to form a planet (at r_0 or further out in the dead zone) that is massive enough to open a gap in the gas disk and thus lead to starvation of the inner gas disk and its depletion via viscous clearing. Strong stellar magnetic fields may truncate the gas disk at a few stellar radii, i.e. $\sim 10R_\odot \sim 0.05$ AU, and this could set an inner limit for Type I migration.

The main prediction of the strong migration scenario is the presence of planets at locations inside the inner dead zone boundary, although this location is uncertain (§2.2) and depends on the disk accretion rate. The implications of the observed KPCs for this scenario are discussed in §3. Next we consider the case of weak migration coupled with efficient growth of planets leading to gap opening.

2.4.2. Gap Opening and Dead Zone Retreat

The process of gap opening by a planet involves it clearing a region over which it has a dominant gravitational influence compared to the star. A planet of mass M_{pl} orbiting in a disk has strong gravitational influence on orbits with impact parameters falling approximately within its Hill sphere, R_H :

$$\begin{aligned} \frac{R_H}{r} &\equiv \left(\frac{M_{\text{pl}}}{3m_*}\right)^{1/3} = \left(\frac{M_R}{3m_*}\right)^{1/3} \\ &\rightarrow 0.0107\phi_{\sigma,0.3}^{2/3}\gamma_{1.4}^{8/15}\kappa_{10}^{2/15}\alpha_{-3}^{-2/15}m_{*,1}^{-7/15} \\ &\quad \times (f_r\dot{m}_{-9})^{4/15}r_{\text{AU}}^{1/15}. \end{aligned} \quad (22)$$

We assume the planet accretes material out to impact parameter $\phi_H R_H$, where $\phi_H \sim 3$ (e.g., Lissauer 1987; Kokubo & Ida 1998). The fractional width of the Toomre unstable ring, λ_T/r , is given by

$$\begin{aligned} \frac{\lambda_T}{r} &= 2\pi Q\sigma_p/v_K \\ &= \frac{3^{1/5}\pi^{3/5}}{2}\phi_{\sigma}k_P Q \left(\frac{\mu}{\gamma k_B}\right)^{-4/5} \left(\frac{\kappa}{\sigma_{\text{SB}}}\right)^{1/5} \alpha^{-1/5} \\ &\quad \times (Gm_*)^{-7/10} (f_r\dot{m})^{2/5} r^{1/10} \\ &\rightarrow 3.41 \times 10^{-3} \phi_{\sigma,0.3} Q \gamma_{1.4}^{4/5} \kappa_{10}^{1/5} \alpha_{-3}^{-1/5} m_{*,1}^{-7/10} \\ &\quad \times (f_r\dot{m}_{-9})^{2/5} r_{\text{AU}}^{1/10}, \end{aligned} \quad (23)$$

which is about a factor of three smaller than R_H/r for all relevant r for our fiducial disk ($R_H/\lambda_T \propto \dot{m}^{-2/15} r^{-1/30}$). Thus after the M_R -mass planet forms from the ring, it will still dominate regions of the disk beyond the initial ring width, and we expect the planet's mass to grow beyond M_R .

We estimate final isolation mass in two ways. First, we evaluate the isolation mass in a pebble-rich disk, $M_{I,p}$, as M_R plus additional accreted mass from sweeping-up a disk with $\Sigma \simeq \Sigma_p$ over impact parameters out to $\phi_H R_H$. This case is relevant if the annular width of the region that had Σ enhanced by pebble drift is $\gtrsim \phi_H R_H$. In this case

$$\begin{aligned} M_{I,p}/M_R &= 1 + \phi_{H,p} R_H (M_{\text{pl}} = M_{I,p})/\lambda_T \\ &\simeq \phi_{H,p} R_H (M_{\text{pl}} = M_{I,p})/\lambda_T, \end{aligned} \quad (24)$$

implying

$$\begin{aligned} M_{I,p} &= \frac{1}{2^{3/2}3^{1/5}\pi^{3/5}} \left(\frac{\phi_{H,p}\phi_{\sigma}k_P}{Q}\right)^{3/2} \left(\frac{\mu}{\gamma k_B}\right)^{-6/5} \\ &\quad \times \left(\frac{\kappa}{\sigma_{\text{SB}}}\right)^{3/10} \alpha^{-3/10} G^{-21/20} m_*^{-1/20} (f_r\dot{m})^{3/5} r^{3/20} \\ &\rightarrow 35.7 \left(\frac{\phi_{H,p,3}\phi_{\sigma,0.3}}{Q}\right)^{3/2} \gamma_{1.4}^{6/5} \kappa_{10}^{3/10} \alpha_{-3}^{-3/10} m_{*,1}^{-1/20} \\ &\quad \times (f_r\dot{m}_{-9})^{3/5} r_{\text{AU}}^{3/20} M_{\oplus}, \end{aligned} \quad (25)$$

where $\phi_{H,p,3} \equiv \phi_{H,p}/3$. The approximation assuming $M_{I,p} \gg M_R$ in Equation 24 is thus verified. $M_{I,p}$ is also shown in Fig. 2. Note that, although these can be close to Jovian-mass planets, they would have approximately terrestrial compositions. As shown below, this mass would also be sufficient to open an isolating gap with the gas disk.

Second, if the width of the pebble-enhanced ($\Sigma = \Sigma_p$) annulus is $\ll \phi_H R_H$, then the isolation mass, $M_{I,g}$, is set by accretion from a gas-dominated disk. The planet needs to first reach mass, M_G , sufficient to open a gas gap. We estimate this via the viscous-thermal criterion

(Lin & Papaloizou 1993),

$$\begin{aligned} M_G &= \frac{\phi_G 40\nu m_*}{r^2 \Omega_K} \\ &= 20 \frac{3^{1/5}}{\pi^{2/5}} \phi_G \left(\frac{\mu}{\gamma k_B}\right)^{-4/5} \left(\frac{\kappa}{\sigma_{\text{SB}}}\right)^{1/5} \\ &\quad \times \alpha^{4/5} G^{-7/10} m_*^{3/10} (f_r\dot{m})^{2/5} r^{1/10} \\ &\rightarrow 5.67 \phi_{G,0.3} \gamma_{1.4}^{4/5} \kappa_{10}^{1/5} \alpha_{-3}^{4/5} m_{*,1}^{3/10} (f_r\dot{m}_{-9})^{2/5} r_{\text{AU}}^{1/10} M_{\oplus}, \end{aligned} \quad (26)$$

where we adopt $\phi_G = 0.3$ based on simulations of (Zhu et al. 2013), who also find ϕ_G depends on net vertical disk B-field strength. The ratio M_R/M_G is given by

$$\begin{aligned} \frac{M_R}{M_G} &= \frac{3^{1/5}\pi^{3/5}}{80} \frac{\phi_{\sigma}^2 k_P^2}{\phi_G} \left(\frac{\mu}{\gamma k_B}\right)^{-4/5} \left(\frac{\kappa}{\sigma_{\text{SB}}}\right)^{1/5} \\ &\quad \times \alpha^{-6/5} (Gm_*)^{-7/10} (f_r\dot{m})^{2/5} r^{1/10} \\ &\rightarrow 0.217 \phi_{G,0.3}^{-1} \phi_{\sigma,0.3}^2 k_P^2 \gamma_{1.4}^{4/5} \kappa_{10}^{1/5} \alpha_{-3}^{-6/5} m_{*,1}^{-7/10} \\ &\quad \times (f_r\dot{m}_{-9})^{2/5} r_{\text{AU}}^{1/10} M_{\oplus}. \end{aligned} \quad (27)$$

Note that both M_G and M_R/M_G are quite sensitive to the value of α , which is quite uncertain, especially at the location relevant for pebble ring formation near the dead zone boundary. Nevertheless, for our fiducial disk $M_R \lesssim M_G$, so we expect that some additional accretion would be needed after formation from the ring mass before a gap could be opened. This phase would allow an opportunity for Type I migration (§2.4.1). If gas is able to cool and join the planet it could also lead to accretion of both gas and pebbles, thus leading to lower density planets. However, given the uncertainties in parameters, such as α , we can also imagine situations where $M_R \gtrsim M_G$, and a gap would be opened simultaneously with planet formation from the pebble ring.

The gaps seen in the simulations of Zhu et al. (2013) (i.e. for $\phi_G \simeq 0.3$) are relatively shallow (deeper gaps will be achieved with larger values of ϕ_G), but still this may be sufficient to allow additional penetration of X-rays that may increase the ionization fraction to activate the MRI and thus cause the pressure maximum associated with the dead zone boundary to move outwards. Such a scenario, discussed below, could lead to a truncation in the supply of pebbles to the planet. This supply may also be impeded by the pressure maximum associated with the outer edge of the gap (e.g., Matsumura & Pudritz 2007).

In the process of opening a deep, well-cleared gap that isolates the planet from further accretion, the planet will likely accrete an additional gas mass by sweeping-up an annulus of a few ($\phi_{H,g}$) Hill radii,

$$\begin{aligned} dM_g &= 2\pi r \phi_{H,g} R_H \Sigma_g \\ &= 2\pi r^2 \phi_{H,g} (M_{\text{pl}}/(3m_*))^{1/3} \Sigma_g, \end{aligned} \quad (28)$$

where Σ_g is given by Equation 17. The final isolation mass of the planet in a gas disk is thus

$$M_{I,g} = \max(M_R, M_G) + dM_g. \quad (29)$$

The solution of the above equation for $M_{I,g}$ for $\phi_{H,g} = 3$ is shown in Fig. 2. For $r_{\text{AU}} \lesssim 1$ there is only a very minor enhancement in mass beyond M_G . For $r_{\text{AU}} \gtrsim 3$, the planet gains most of its eventual mass in these final

stages of opening a gas gap. These considerations suggest that $M_R/M_{I,g}$ declines with radius, so that outer planets will tend to be of lower density.

Once the first planet has formed and opened a gap, we expect that interior disk material, which is mostly in an MRI-active region, will rapidly accrete on a local viscous time. The dead zone boundary should then retreat outwards, since protostellar X-rays will now be able to penetrate further. The same processes that formed the first planet, i.e. collection of pebbles at a pressure maximum, should then operate to form a second planet, assuming there is still a supply of pebbles from the outer disk.

The pressure maximum associated with the first planet's outer gap edge sets a minimum separation of the location of the next planet to be $\sim \phi_H R_H$. However, if the MRI-active, inner disk makes a transition to being completely cleared, then we expect a large reduction in the absorbing column and thus perhaps a large shift in the location of the dead zone inner boundary, especially relative to $\phi_H R_H$, since $\phi_H R_H/r \ll 1$. An accurate estimate of the distance of dead zone retreat would involve a sophisticated calculation of the ionization, thermal and magnetic field structure of the disk, as a gap and inner hole are established. We defer such a calculation to a future paper and for the moment simply assume a new dead zone inner boundary pressure maximum will be established at least $\phi_H R_H$ from the first planet but likely significantly further.

Assuming a steady disk accretion rate and constant value of α , the masses of planets forming from an initially gravitationally unstable ring should follow the radial dependencies of Equation 26 ($M_{I,g} \simeq M_G \propto r^{1/10}$ for $r \lesssim 1$ AU) for isolation in a gas-dominated disk where $M_G > M_R$. If $M_R > M_G$, then the mass scaling with radius would be expected to follow Equation 20 ($M_{I,g} \simeq M_R \propto r^{1/5}$ for $r \lesssim 1$ AU). In a pebble-dominated disk, then the masses would be described by Equation 25 ($M_{I,p} \propto r^{3/20}$): these masses tend to always be enough to open a gap. These are all similar, relatively flat scalings with the orbital radius. These dependencies can be tested against observed planetary systems (§3), but with the caveat that there is the possibility of the efficient Type I migration scenario (§2.4.1), in which planetary orbits are shrunk from the location of the parent pebble ring.

2.4.3. Constraints from the Global Disk Pebble Reservoir

In either limit of efficient or inefficient Type I migration, subsequent planet formation requires continued pebble drift to r_0 , which will be reduced once the reservoir of disk solids is depleted. The mass in solids initially contained in the gas disk within radius $r_1 \gg r_0$ is

$$\begin{aligned} M_s(< r_1) &= \int^{r_1} f_s 2\pi r \Sigma_g dr \\ &= \frac{20\pi^{2/5}}{3^{6/57}} f_s \left(\frac{\mu}{\gamma k_B}\right)^{4/5} \left(\frac{\kappa}{\sigma_{SB}}\right)^{-1/5} \alpha^{-4/5} \\ &\quad \times (Gm_*)^{1/5} \dot{m}^{3/5} r_1^{7/5} \\ &\rightarrow 0.178 f_{s,-2} \gamma_{1.4}^{-4/5} \kappa_{10}^{1/5} \alpha_{-3}^{-4/5} m_{*,1}^{1/5} \dot{m}_{-9}^{3/5} r_{1,AU}^{7/5} M_\oplus. \end{aligned} \quad (30)$$

Assuming the first planet forms with mass $M_R = \epsilon_p M_s(< r_1)$ with efficiency $\epsilon_p = 0.5$, we estimate the

radius r_1 that becomes depleted of pebbles:

$$\begin{aligned} r_1 &= \left(\frac{7}{5}\right)^{5/7} \frac{3^{8/7}}{2^{20/7} \pi^{1/7}} \frac{(\phi_\sigma k_P)^{10/7}}{(f_s \epsilon_p)^{5/7}} \left(\frac{\mu}{\gamma k_B}\right)^{-12/7} \left(\frac{\kappa}{\sigma_{SB}}\right)^{3/7} \\ &\quad \times \alpha^{2/7} G^{-8/7} m_*^{-3/7} \dot{m}^{1/7} r_0^{1/7} \\ &\rightarrow 6.55 \frac{\phi_{\sigma,0.3}^{10/7} \gamma_{1.4}^{12/7} \kappa_{10}^{3/7}}{(f_{s,0.01} \epsilon_{p,0.5})^{5/7}} \alpha_{-3}^{2/7} m_{*,1}^{-3/7} \dot{m}_{-9}^{1/7} r_{0,AU}^{1/7} \text{ AU}. \end{aligned} \quad (31)$$

Note we have adopted a single value of α for the disk out to r_1 . If the dead zone outer boundary has a radial extent $< r_1$, then this estimate would need to be modified, leading to an increased value of α in the outer region and thus a larger value of r_1 . Equation 31 shows that a fairly large region of the disk is needed to supply the mass of pebbles to form a Toomre ring mass planet, comparable to the outer scales predicted for dead zones (e.g., Mohanty et al. 2013; Dzyurkevich et al. 2013). Formation of a series of super-Earth mass planets from pebbles could require initial protoplanetary disks extending to ~ 100 AU.

Pebble drift can also be reduced if an outer planet forms, e.g., via regular core accretion, gaseous gravitational instability, or gravitational instability of an outer pebble ring captured in a local pressure maximum. If massive enough, such a planet would interrupt the supply of pebbles, i.e., they would be depleted from the disk interior to this planet. However, we expect regular core accretion in the outer disk to be slower than pebble drift to the inner region, and indeed inhibited by pebble drift. Gaseous gravitational instability is unlikely to operate within ~ 10 – 100 AU unless disks are very massive (e.g., Rafikov 2005). If an outer pebble ring forms first before an inner ring is established at r_0 , then that process can be viewed as a scaled-up version of the theory presented here. Outer pebble ring formation may be induced by pressure maxima induced by sudden opacity changes (Drazkowska et al. 2013; Boley & Ford 2013, e.g. at ice lines) or MRI activity changes (e.g., due to gas-phase metal freeze out; Dzyurkevich et al. 2013). The relative efficiency of inner versus outer pebble ring formation may depend sensitively on disk properties, including \dot{m} and initial magnetization, leading to distinct classes of planetary systems, e.g. STIPs versus Solar-System analogs.

Once inside-out planet formation via pebble rings finishes, much of the remaining gas in the disk will be likely accreted by the outermost planet, eventually crossing its gap (e.g., Uribe et al. 2013), to form a gas giant, which would then deviate from the above analytic $M_{pl} - r$ relations.

3. COMPARISON TO KEPLER SYSTEMS

Figure 3a shows M_R , M_G , $M_{I,g}$, and $M_{I,p}$ for $\dot{m} = 10^{-10}$, 10^{-9} and $10^{-8} M_\odot \text{ yr}^{-1}$ together with the KPCs, whose masses are crudely estimated using a power-law $M_{pl} = M_\oplus (R_{pl}/R_\oplus)^{2.06}$ (Lissauer et al. 2011). Focusing on STIPs, we discard planets with $R_{pl} \geq 10 R_\oplus$ (none are in multi-transiting systems). The estimated KPC masses are similar to those expected from the fiducial model of inside-out planet formation. However, since $M_{I,g} \simeq M_R \propto \dot{m}^{4/5}$ (Equation 20) or $M_{I,g} \simeq M_G \propto \dot{m}^{2/5}$ (Equation 26) and $M_{I,p} \propto \dot{m}^{3/5}$ (Equation 25), a range in masses could occur at a given r if \dot{m} varies. Such

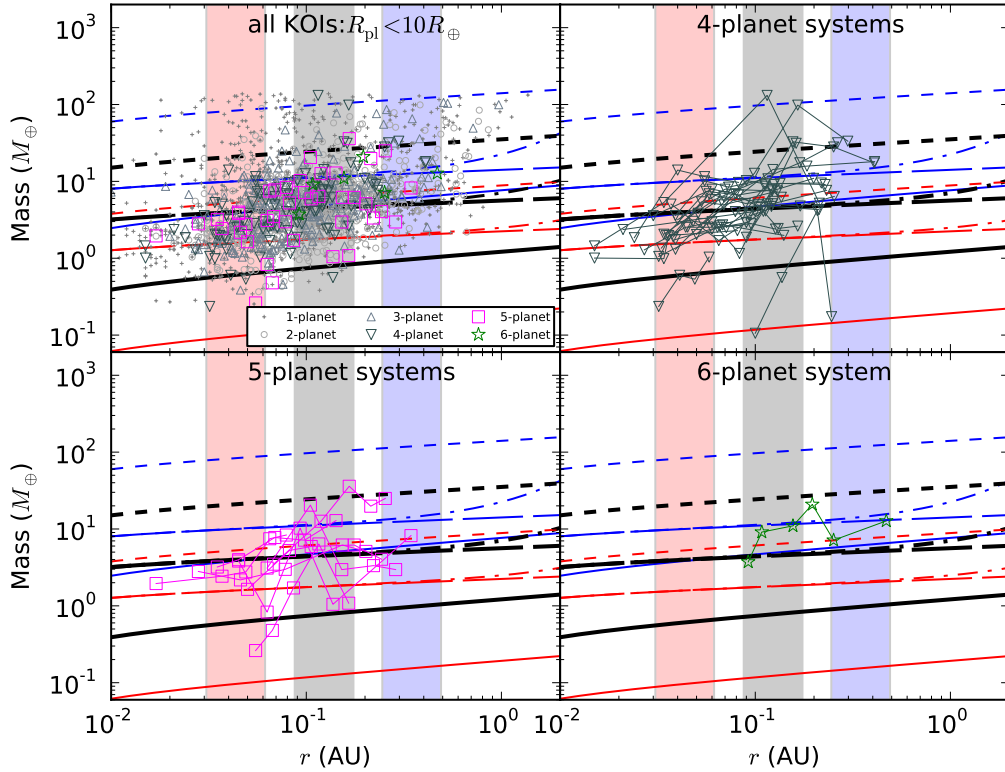


FIG. 3.— Lines and shaded regions have the same meaning as in Figure 2, but zoomed to a narrower mass range. (a) Top-left: KPCs with $R_{\text{pl}} < 10 R_{\oplus}$ are shown from Batalha et al. (2013) (16-month data release). (b) Top-right: Only 4-planet systems are shown. (c) Bottom-left: Only 5-planet systems are shown. (d) Bottom-right: Only the 6-planet system is shown. Note, here the KPC masses are approximate estimates using a simple scaling-law with radius (see text).

variation is expected from system to system and even over time within a given system during planet formation.

Radial dependence of relative planetary masses in a given system provides a more powerful test, since this removes some systematic uncertainties resulting from system to system variation, such as m_* and perhaps some dispersion in \dot{m} . The twenty-eight 4-planet systems, the eight 5-planet systems and the single 6-planet system are shown in Figs. 3 b, c, and d, respectively. Fitting a power-law $M_{\text{pl}} \propto r^{k_M}$ to these individual systems, we find $k_M = 0.92 \pm 0.63, 0.78 \pm 0.64, 0.50$ for the 4, 5, 6-planet systems (uncertainty reflects sample dispersion), respectively. These results are consistent with the theoretical predictions, with caveats that there may be large systematic errors in these mass estimates and current orbits may differ from formation orbits due to migration.

Some KPCs are observed interior to the estimated dead-zone boundaries in our fiducial disk model (Figure 3), although these locations are quite uncertain. This would imply that some degree of migration has occurred, such as described in §2.4.1 or after gap opening, via Type II migration.

A subset of the KPCs have directly measured masses, primarily by transit timing variations (TTV; e.g., Butler et al. 2006; Holman et al. 2010; Cochran et al. 2011; Carter et al. 2012; Gautier et al. 2012; Lissauer et al.

2013). Figure 4 shows the theoretical $M_{\text{pl}} - r$ relations along with these systems (see also Table 1). Averaging these 6 systems, $k_M = 1.0 \pm 2.1$. Averaging all adjacent pairs, $k_M = 0.47 \pm 2.7$. These values are consistent with scalings for $M_{I,g} \simeq M_G$ ($k_M = 0.1$ for $r \lesssim 1$ AU) or $M_{I,p}$ ($k_M = 0.15$), but more data are required for a more stringent test. There is a real and significant dispersion in the values of k_M seen in adjacent planetary pairs within the systems with ≥ 3 planets, which, in the context of inside-out planet formation, would require variation of \dot{m} of factors of a few during formation of the system.

Planetary densities show wide dispersion, but a tendency to decrease with r (Table 1). Some relatively low densities are seen, which would require $M_{\text{pl}} \gg M_R$ and imply that gas accretion could occur onto the initial core. Even for higher density systems, models of rocky cores surrounded by residual H/He atmospheres are needed for comparison of the theory with these data. Evolution due to atmospheric evaporation may also complicate such comparisons (Owen & Wu 2013).

Finally we consider orbital spacings between adjacent planets via $\phi_{\Delta r, i} \equiv \Delta r_i / R_{H, i}$, where $\Delta r_i = r_{i+1} - r_i$ and $R_{H, i}$ is the Hill radius of the inner planet of the pair. The distributions of the large KPC sample are shown in Figure 5, with a broad distribution peaking at $\phi_{\Delta r} \sim 20$ –

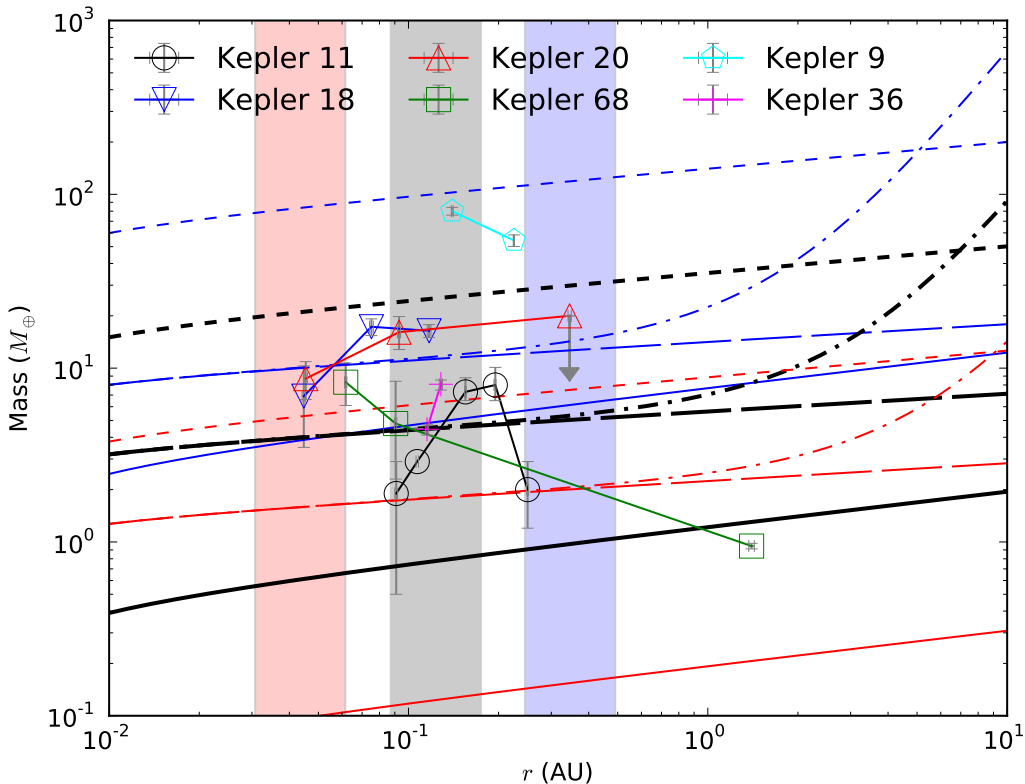


FIG. 4.— Similar to Figure 3, but showing the 6 *Kepler* systems with direct mass measurements.

50. The values for the TTV systems are listed in Table 1 and are similar, with $\phi_{\Delta r} \gtrsim 10$ and 4 of the 12 values clustered at $\phi_{\Delta r} \simeq 14$. Thus $\phi_{\Delta r}$ is typically at least several times greater than our fiducial value of $\phi_H = 3$ for gap opening, consistent with our theoretical expectations that the spacing is determined not via dynamical stability considerations (through $\phi_H R_H$) but via retreat of the dead zone and associated location of the pressure maximum. However, it is also possible that these spacings may be influenced by migration.

If $\phi_{\Delta r}$ is set by dead zone retreat one may expect greater relative change immediately after formation of the first planet, since this is the first gap-opening episode in the disk. Comparing $\phi_{\Delta r}$ distributions in systems with $N_p \geq 3, 4, 5$ planets (minimal detection bias is expected for interior planet locations), indeed $\phi_{\Delta r,1}$ tends to be larger than $\phi_{\Delta r,2}$ and $\phi_{\Delta r,3}$. For $N_p \geq 3$ -sample, the KS test gives 9×10^{-5} probability that $(\phi_{\Delta r,1}, \phi_{\Delta r,2})$ are drawn from the same distribution. Equivalent probabilities for $N_p \geq 4$ -sample for $(\phi_{\Delta r,1}, \phi_{\Delta r,2})$, $(\phi_{\Delta r,1}, \phi_{\Delta r,3})$, $(\phi_{\Delta r,2}, \phi_{\Delta r,3})$ are 2×10^{-4} , 5×10^{-4} , 0.8, respectively.

4. DISCUSSION AND SUMMARY

We have presented a simple theoretical model of “inside-out” planet formation: pebbles form and drift to the inner disk; they accumulate and dominate in a ring at the pressure maximum associated with the inner dead zone boundary; a $\sim 1 M_{\oplus}$ planet forms, perhaps initi-

ated by gravitational instability of the ring; inward Type I migration may bring the planet inside the MRI-active region, allowing a new ring and planet to form at the dead zone boundary; under certain conditions a planet may form that is massive enough to isolate itself from the disk by opening a deep gap; more typically, and if Type I migration is inefficient, gap-opening would require the planet to accrete additional mass (pebbles and/or gas); a variety of mean planetary densities can arise, depending on the relative importance of residual gas accretion; gap opening allows greater X-ray penetration and the dead zone retreats; for a dead zone boundary set by thermal ionization, a simple gradual reduction in accretion rate would also lead to dead zone retreat; planet formation proceeds sequentially, one at a time, from a series of retreating pebble rings, as long as the supply of pebbles is maintained from the outer disk.

The *Kepler* STIPs planetary masses and relative orbital spacings are consistent with expectations from this simple theoretical model, for typical disk accretion rates $\sim 10^{-9} M_{\odot} \text{ yr}^{-1}$. The observed $M_{\text{pl}} - r$ relationship agrees with the theoretical expectation, although more data are needed to improve this test. Observed dispersion of this relation within individual systems may indicate accretion rate variability by factors of several during planet formation.

Investigation of this model can be improved in several ways, including (1) a more accurate calculation of disk

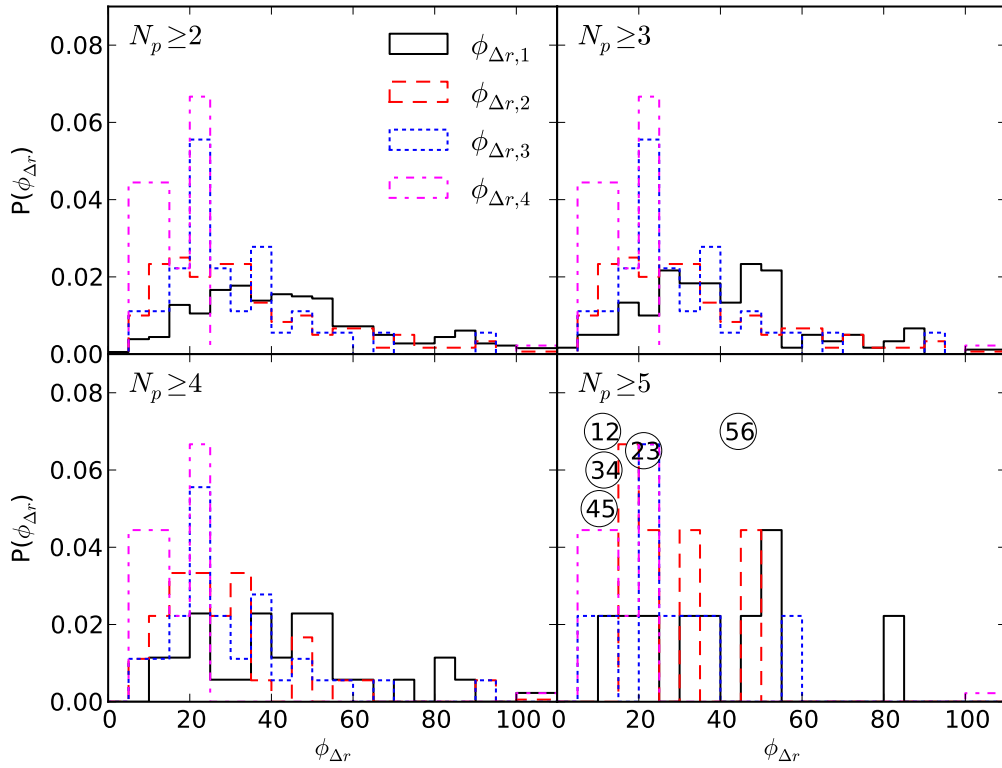


FIG. 5.— Probability distribution of $\phi_{\Delta r}$ for KPC systems with $N_p \geq 2$ (top-left), 3 (top-right), 4 (bottom-left), and 5 (bottom-right). The $\phi_{\Delta r}$ values for the 6-planet system are shown with inscribed circles in the bottom-right panel. Solid (black), dashed (red), dotted (blue), and dash-dot (magenta) lines show $\phi_{\Delta r,1}$ (separation between planets 1–2), to $\phi_{\Delta r,4}$ (separation between planets 4–5), respectively. Planets are indexed with increasing distance from the star.

structure that allows for realistic opacity variations and heating from the central star; (2) an estimate of the dead zone inner boundary involving an explicit calculation of the ionization fraction; (3) a dynamical model that tracks pebble formation, growth, and radial drift (potentially subject to secular instabilities leading to planetesimal formation, Goodman & Pindor 2000) to form a pebble ring; (4) a dynamical model for planet formation from such a pebble ring, which dominates the local mass surface density of the disk, and especially its propensity to form a single massive planet (cf. Johansen et al. 2007, 2009; Bai & Stone 2010a,b, who investigated formation of clumps of solids from more gas-rich initial conditions mediated by hydrodynamic streaming instabilities and vortices); (5) numerical investigation of migration, subsequent accretion and gap-opening to the isolation mass (e.g., Zhu et al. 2013), and resulting dead zone retreat. Improved observational tests require better measurements of planetary masses and densities. The dispersion in orbital inclination angles may provide additional constraints that can help distinguish inside-out planet formation from other formation models, such as formation from an inner enriched disk or outer-disk formation followed by long-distance migration.

The model of inside-out planet formation requires a sufficiently high rate of supply of pebbles to the inner

disk. The observed diversity of planetary system architectures, from STIPs to that of our own Solar System, may result from variations in both the efficiency with which pebbles form and, once formed, their ability to drift radially inwards through the disk without interruption. Formation rate of pebbles is potentially related to the temperature structure and the prevalence of icy dust grain mantles in the bulk of the disk during the late stages of star formation. Future studies of the processes that lead to variation in inner disk pebble supply rate are also needed.

We thank Aaron Boley, Eric Ford, Brad Hansen, Anders Johansen, Greg Laughlin, Subu Mohanty, Ralph Pudritz, Andrew Youdin, Yichen Zhang, Jeremy Goodman, Zhaohuan Zhu, Roman Rafikov, Scott Tremaine, and Leonardo Testi for helpful discussions. SC acknowledges NASA grants NNX08AR04G, NNX12AF73G and the UF Theory Postdoctoral Fellowship. JCT acknowledges NASA grants ATP09-0094, ADAP10-0110.

TABLE 1
 KPC SYSTEMS WITH DIRECT MASS MEASUREMENTS.

Planet ^a Name	R_{pl} (R_{\oplus})	M_{pl} (M_{\oplus})	ρ_{pl} (gcm^{-3})	r (AU)	$\phi_{\Delta r}$ ^b	k_M ^c Adjacent Pairs	k_M ^d System
Kepler-9b	9.22 ± 0.8	80 ± 4	0.524 ± 0.132	0.140 ± 0.001	14 ± 1	-0.8	-0.8
Kepler-9c	9.01 ± 0.7	54 ± 4	0.383 ± 0.098	0.225 ± 0.001	-	-	-
Kepler-11b	1.8 ± 0.02	$1.9^{+1.4}_{-1.0}$	$1.77^{+1.29}_{-0.94}$	0.091 ± 0.001	14 ± 5	2.6	0.5
Kepler-11c	$2.87^{+0.01}_{-0.02}$	$2.9^{+2.9}_{-1.6}$	$0.68^{+0.68}_{-0.36}$	0.107 ± 0.001	31 ± 10	2.5	-
Kepler-11d	3.11 ± 0.02	$7.3^{+0.8}_{-1.5}$	$1.33^{+0.15}_{-0.28}$	0.155 ± 0.001	13 ± 2	0.4	-
Kepler-11e	4.18 ± 0.02	$8.0^{+1.5}_{-2.1}$	$0.60^{+0.12}_{-0.16}$	$0.195^{+0.002}_{-0.001}$	14 ± 2	-5.6	-
Kepler-11f	$2.48^{+0.02}_{-0.03}$	$2.0^{+0.8}_{-0.9}$	$0.73^{+0.30}_{-0.34}$	0.250 ± 0.002	-	-	-
Kepler-18b	2.0 ± 0.1	6.9 ± 3.4	4.9 ± 2.4	0.0447 ± 0.0006	35 ± 9	1.8	0.9
Kepler-18c	5.49 ± 0.26	17.3 ± 1.9	0.59 ± 0.07	0.0752 ± 0.0011	21 ± 3	-0.1	-
Kepler-18d	6.98 ± 0.33	16.4 ± 1.4	0.27 ± 0.03	0.1172 ± 0.0017	-	-	-
Kepler-20b	$1.91^{+0.12}_{-0.21}$	$8.7^{+2.1}_{-2.2}$	$6.5^{+2.0}_{-2.7}$	$0.04537^{+0.00054}_{-0.00060}$	49 ± 7	0.8	0.4
Kepler-20c	$3.07^{+0.20}_{-0.31}$	$16.1^{+3.3}_{-3.7}$	$2.91^{+0.85}_{-1.08}$	0.0930 ± 0.0011	104 ± 12	-	-
Kepler-20d	$2.75^{+0.17}_{-0.30}$	< 20	< 4.07	$0.3453^{+0.0041}_{-0.0046}$	-	-	-
Kepler-36b	1.486 ± 0.035	$4.45^{+0.33}_{-0.27}$	$7.46^{+0.74}_{-0.59}$	0.1153 ± 0.0015	7 ± 2	5.6	5.6
Kepler-36c	3.679 ± 0.054	$8.08^{+0.60}_{-0.46}$	$0.89^{+0.07}_{-0.05}$	0.1283 ± 0.0016	-	-	-
Kepler-68b	$2.31^{+0.06}_{-0.09}$	$8.3^{+2.2}_{-2.4}$	$3.32^{+0.86}_{-0.98}$	0.06170 ± 0.00056	23 ± 4	-1.4	-0.6
Kepler-68c	$0.953^{+0.037}_{-0.042}$	$4.8^{+2.5}_{-3.6}$	28^{+13}_{-23}	0.09059 ± 0.00082	878 ± 228	-0.6	-
Kepler-68d	-	0.947 ± 0.035^e	-	1.4 ± 0.03	-	-	-

^aData for Kepler-9,11,18,20,36,68 from Holman et al. (2010); Lissauer et al. (2013); Cochran et al. (2011); Gautier et al. (2012); Carter et al. (2012); Gilliland et al. (2013), respectively.

^b $\phi_{\Delta r} = (r_{i+1} - r_i)/R_{H,i}$.

^c $M_{\text{pl}} \propto r^{k_M}$ fitted for adjacent pairs.

^d $M_{\text{pl}} \propto r^{k_M}$ fitted for whole system.

^eRadial velocity measurement of $M_{\text{pl}} \sin i$.

REFERENCES

- Armitage, P. J. 2007, arXiv:astro-ph/0701485
- Bai, X. N. & Stone, J. M. 2010a, *ApJ*, 722, 220
- Bai, X. N. & Stone, J. M. 2010b, *ApJ*, 722, 1437
- Batalha, N. M., Rowe, J. F., Bryson, S. T. et al. 2013, *ApJS*, 204, 24
- Batygin, K., & Morbidelli, A. 2013, *AJ*, 145, 1
- Blum, J. 2010, *Research in Astronomy and Astrophysics*, 10, 1199
- Boley, A. C. & Ford, E. B. 2013, arXiv:1306.0566[astro-ph.EP]
- Butler, R. P., Wright, J. T., Marcy, G. W. et al. 2006, *ApJ*, 646, 505
- Carter, J. A., Agol, E., Chaplin, W. J. et al. 2012, *Science*, 337, 556
- Chatterjee, S., Ford, E. B., Matsumura, S., & Rasio, F. A. 2008, *ApJ*, 686, 580
- Chiang, E. & Laughlin, G. 2013, *MNRAS*, 431, 3444
- Cochran, W. D., Fabrycky, D. C., Torres, G. et al. 2011, *ApJS*, 197, 7
- Drazkowska, J., Windmark, F., & Dullemond, C. P. 2013, arXiv:1306.3412[astro-ph.EP]
- Dzyurkevich, N., Flock, M., Turner, N. J., Klahr, H., & Henning, T. 2010, *A&A*, 515, A70
- Dzyurkevich, N., Turner, N. J., Henning, T., & Kley, W. 2013, *ApJ*, 765, 114
- Fang, J. & Margot, J. L. 2012, *ApJ*, 761, 92
- Frank, J., King, A. & Raine, D. J., 2002, *Accretion Power in Astrophysics: Third Edition* (Cambridge University Press; ISBN 0521620538)
- Gautier, III, T. N., Charbonneau, D., Rowe, J. F. et al. 2012, *ApJ*, 749, 15
- Gilliland, R. L., Marcy, G. W., Rowe, J. F. et al. 2013, *ApJ*, 766, 40
- Goodman, J. & Pindor, B. 2000, *Icarus*, 148, 537
- Goodman, J. & Rafikov, R. R. 2001, *ApJ*, 552, 793
- Hansen, B. & Murray, N. 2013, arXiv:1301.7431
- Hansen, B. M. S. & Murray, N. 2012, *ApJ*, 751, 158
- Holman, M. J., Fabrycky, D. C., Ragozzine, D. et al. 2010, *Science*, 330, 51
- Johansen, A., Oishi, J. S., Mac Low, M. M., Klahr, H., Henning, T., & Youdin, A. 2007, *Nature*, 448, 1022
- Johansen, A., Youdin, A., & Mac Low, M. M. 2009, *ApJ*, 704, 75
- Kley, W., & Nelson, R. P. 2012, *ARA&A*, 50, 211
- Kokubo, E. & Ida, S. 1998, *Icarus*, 131, 171
- Lin, D. N. C. & Papaloizou, J. C. B. 1993, in *Protostars and Planets III*, ed. E. H. Levy & J. I. Lunine (Tucson: Univ. Arizona Press), 749
- Lissauer, J. J. 1987, *Icarus*, 69, 249
- Lissauer, J. J., Jontof-Hutter, D., Rowe, J. F. et al. 2013, arXiv:1303.0227.astro-ph.EP
- Lissauer, J. J., Ragozzine, D., Fabrycky, D. C. et al. 2011, *ApJS*, 197, 8
- Lithwick, Y. & Wu, Y. 2012, *ApJ*, 756, 11
- Lubow, S. H. & Ida, S. 2011, *Exoplanets*, Ed. Seager, S. (University of Arizona Press, 2011)
- Lyra, W. & Mac Low, M. M. 2012, *ApJ*, 756, 62L
- Matsumura, S., & Pudritz, R. E. 2005, *ApJ*, 618, 137
- Matsumura, S., & Pudritz, R. E. 2007, *ApJ*, 660, 1609
- Meheut, H., Meliani, Z., Varniere, P. & Benz, W. 2012, *A&A*, 545, 134
- Menou, K. & Goodman, J. 2004, *ApJ*, 606, 520
- Mohanty, S., Ercolano, B., & Turner, N. J. 2013, *ApJ*, 764, 65
- Nagasawa, M. & Ida, S. 2011, *ApJ*, 742, 72
- Ormel, C. & Okuzumi, S. 2013, arXiv:1305.1890. astro-ph.EP
- Owen, J. E. & Wu, Y. 2013, arXiv:1303.3899.astro-ph.EP
- Paardekooper, S. J., & Mellema, G. 2006, *A&A*, 459, 17
- Paardekooper, S. J., Baruteau, C., Crida, A., & Kley, W. 2010, *MNRAS*, 401, 1950
- Rafikov, R. R. 2005, *ApJ*, 621, 69
- Rasio, F. A. & Ford, E. B. 1996, *Science*, 274, 954
- Rein, H. 2012, *MNRAS*, 427, 21
- Shakura, N. I. & Sunyaev, R. A. 1973, *A&A*, 24, 337
- Takeuchi, T., & Lin, D. N. C. 2002, *ApJ*, 581, 1344
- Umebayashi, T. & Nakano, T. 1988, *Progress of Theoretical Physics Supplement*, 96, 151
- Uribe, A. L., Klahr, H., & Henning, T. 2013, *ApJ*, 769, 97
- Varnière, P., & Tagger, M. 2006, *A&A*, 446, 13
- Ward, W. R. 1997, *Icarus*, 126, 261
- Weidenschilling, S. J. 1977, *MNRAS*, 180, 57
- Weidenschilling, S. J. 1980, *Icarus*, 44, 172
- Williams, J. P. & Cieza, L. A. 2011, *ARA&A*, 49, 67
- Wood, K., Wolff, M. J., Bjorkman, J. E., & Whitney, B. 2002, *ApJ*, 564, 887
- Youdin, A. N. & Shu, F. H. 2002, *ApJ*, 580, 494
- Youdin, A. N. & Goodman, J. 2005, *ApJ*, 620, 459
- Youdin, A. N. & Kenyon, S. J. *From Disks to Planets*, ed. T. D. Oswalt, L. M. French, & P. Kalas, 1
- Zhang, Y., Tan, J. C., & McKee, C. F. 2013, *ApJ*, 766, 86
- Zhu, Z., Stone, J. M., & Rafikov, R. R. 2013, *ApJ*, 768, 143